INORGANIC CHEMISTRY
FRONTIERS

RESEARCH ARTICLE

View Article Online
View Journal

Published on 21 February 2018. Downloaded by KING SAUD UNIVERSITY LIBRARIES on 04/04/2018 08:24:15.

Check for updates

Cite this: DOI: 10.1039/c7qi00799j

Hierarchically structured $CuFe_2O_4$ ND@RGO composite for the detection of oxidative stress biomarker in biological fluids

Shen-Ming Chen,[a] Rajaji Umamaheswari,[a] Govindasamy Mani,[b] Tse-Wei Chen,[a] M. Ajmal Ali,[*b] Al-Hemaid Fahad M. A.,[b] M. S. Elshikh[b] and M. Abul Farah[c]

In this work, stable and catalytically active copper ferrite nanodots ($CuFe_2O_4$) entrapped by porous RGO nanosheets were prepared *via* a facile condensation process using a green reducing agent. The composite was characterized by HR-TEM, EDX, XRD, Raman, TGA, and electrochemical methods. Oxidative stress caused by the imbalance between oxidants and antioxidant defenses is implicated in many pathological conditions including age-related disorders, cancer, and cardiovascular, inflammatory, neurodegenerative and neuropsychiatric diseases. 3-Nitrotyrosine is an electrochemically active biomarker of oxidative stress; hence its electrochemical determination is useful to set up a sensitive analytical tool for oxidative stress measurement. The electrocatalytic activities of a $CuFe_2O_4$@RGO composite modified electrode toward 3-nitrotyrosine were studied in detail. A rapid, sensitive, selective and reproducible electrochemical sensing platform was developed for the detection and quantification of 3-nitrotyrosine under neutral pH conditions. Remarkably, the limit of detection was found to be 25.14 pM, which surpassed the detection limits of many existing analytical methods. The practical applicability of the method was demonstrated in human urine and blood serum samples.

Received 16th December 2017,
Accepted 21st February 2018

DOI: 10.1039/c7qi00799j

rsc.li/frontiers-inorganic

1. Introduction

Oxidative stress plays a prominent role in many pathological conditions; hence, it is vital to develop a reliable analytical device for monitoring its progress in our bodies.[1–3] 3-Nitrotyrosine (3-NT) is one of the important biomarkers of oxidative stress. It is a product of tyrosine nitration mediated by reactive nitrogen species (RNS) such as nitrogen dioxide and peroxynitrite.[3–7] Elevated levels of 3-NT in biological fluids are an indicator of oxidative stress. For 3-NT detection, methods such as high-performance liquid chromatography (HPLC),[8] atomic fluorescence spectrometry,[9] luminol-mediated chemiluminescence,[10] capillary electrophoresis,[11] and flow injection analysis[2] have been developed. However, many of these methods are laborious, bulky, expensive, and time-consuming. Taking advantage of exceptional traits, such as being easy-to-operate, low-cost, portable, sensitive, and simple-to-fabricate, herein, we aim to develop an electrochemical sensing method for the detection and quantification of 3-NT released in biological fluids.[12–15] Reduced graphene oxide (RGO) based nanocomposite modified electrodes display excellent electrocatalytic ability, a large surface area, high conductivity and unique mechanical vigor.[16–18]

Hence, they are widely used in fabricating electrochemical sensor devices.[19–21] Besides, many transition metal oxide-hydroxide material based nanomaterials have been developed for electrochemical applications.[22–24] Particularly, copper and iron based nanomaterials are widely utilized in electrocatalysis attributed to their excellent electronic properties, voluminous surface area, as well as high capability.[25,26]

Here, we have synthesized copper ferrite nanodots ($CuFe_2O_4$) and $CuFe_2O_4$ nanodots supported on porous RGO nanomaterials through a simple solution-phase condensation method for electrochemical sensor applications (Scheme 1). For the first time, we have developed a multi-conventional screen-printed carbon electrode (MSPE) modified with $CuFe_2O_4$@RGO nanosheets as an electrochemical probe for the highly selective and sensitive monitoring of 3-NT. Cyclic voltammetry (CV) and amperometric methods are used as

[a]*Department of Chemical Engineering and Biotechnology, National Taipei University of Technology, No. 1, Section 3, Chung-Hsiao East Road, Taipei 106, Taiwan*
[b]*Department of Botany and Microbiology, College of Science, King Saud University, Riyadh-11451, Saudi Arabia. E-mail: majmalaliksu@gmail.com*
[c]*Department of Zoology, College of Science, King Saud University, Riyadh-11451, Saudi Arabia*

Published on 21 February 2018. Downloaded by KING SAUD UNIVERSITY LIBRARIES on 04/04/2018 08:24:15.

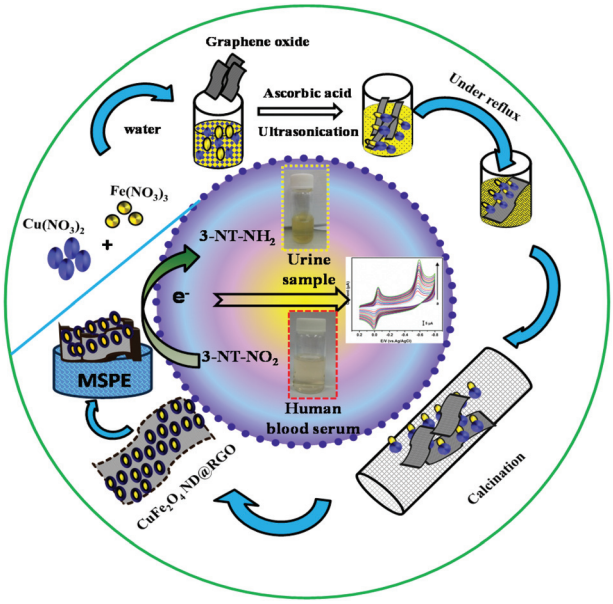

Scheme 1 Schematic representation of the green synthesis of $CuFe_2O_4$ nanodots incorporated on porous RGO sheets and electrochemical determination of oxidative stress biomarker in human urine and blood samples.

signal read outs. Our study found that $CuFe_2O_4$@RGO/MSPE has excellent sensing capability to 3-NT released in human urine and blood serum samples.

2. Experimental

2.1. Chemicals, apparatus, and methods

Graphite, $Cu(NO_3)_2{\cdot}6H_2O$, and $Fe(NO_3)_3{\cdot}9H_2O$ were purchased from Merck. All the other chemicals were acquired from Sigma-Aldrich and used as received. Double distilled water was used for all the experiments. 0.1 M phosphate buffer (PB) solution was used as the supporting electrolyte, which was prepared from sodium dihydrogen phosphate, and disodium hydrogen phosphate. Human serum was acquired from Chang Gung University, Taiwan, while the research protocols were approved by the Institutional Animal Ethic Committee. The real sample analysis performed in human serum sample was performed in compliance with the laws and institutional guidelines of Chang Gung University, Taiwan.

Electrochemical studies were performed on a multi-conventional screen-printed electrode (MSPE) (Bioanalytical Systems, Inc., USA), in which the nanocomposite modified carbon surface acted as a working electrode (carbon-area 0.071 cm^2), Ag|AgCl as a reference electrode and platinum as a counter electrode. The CHI 1205b electrochemical workstation (CH Instruments, Inc., U.S.A) was used to perform all the electrochemical measurements. Prior to each electrochemical experiment, the electrolyte solutions were deoxygenated with pre-purified flow of nitrogen gas for 30 min unless otherwise specified. Surface morphological studies were carried out using a high-resolution transmission electron microscope (HR-TEM) (H-7600, Hitachi, Japan). Raman spectra were acquired using a micro-spectrometer (Renishaw inVia system, UK) with a 514.4 nm He/Ne laser. X-ray diffraction (XRD) studies were performed using an XPERT-PRO (PANalytical B.V., the Netherlands) diffractometer (Cu Kα radiation, k = 1.54 Å). EIM6ex Zahner (Kronach, Germany) was used for electrochemical impedance spectroscopy (EIS) studies. TGA was performed on a Netzsch TG-209 instrument under an air atmosphere.

2.2. Preparation of graphene oxide (GO)

200 mg of graphite was added to 100 mL of H_2SO_4 and H_3PO_4 mixture (4 : 1) solution, under stirring. Next, the whole mixture was heated at 70 °C for 1 h, and then the mixture was cooled to room temperature.[27,28] Then the mixture was transferred to 150 mL of ice containing 20 mL H_2O_2 (30%). The obtained brown coloured sediment was filtered and washed 3 times with HCl (20 vol%, 100 mL each), 2 times with ethanol (20 mL each, 100 mL each) and 2 times with ether (20 mL each, 100 mL each). Finally, the purified graphite oxide was freeze-dried. Subsequently, the graphite oxide was exfoliated to graphene oxide (GO) *via* ultrasonication at 4000 rpm for 1 h.

2.3. Synthesis of a $CuFe_2O_4$ ND@RGO composite

A $CuFe_2O_4$ ND@RGO composite was synthesized as follows. First, 0.288 g $Cu(NO_3)_2{\cdot}6H_2O$, and 0.962 g $Fe(NO_3)_3{\cdot}9H_2O$ were pre-mixed together in the presence of 30 mL distilled water to yield a homogeneous mixture. Afterwards, 25 mg GO (in 20 mL water) was added to the above solution and ultrasonicated for 30 min. Subsequently, 5.2836 g (1 M) ascorbic acid was added and the whole mixture was refluxed at 75 °C under stirring. Here, ascorbic acid was added as a reducing agent to reduce GO to RGO. After cooling down, the solid products were recovered by filtration, and dried in an oven at 75 °C. Then, the solid was calcinated in a tubular furnace at a temperature of 750 °C for 7 h under an air atmosphere, wherein the heating rate was 2 °C min^{-1}. Finally, a brown colored powder was obtained, which was named a $CuFe_2O_4$@RGO nanocomposite.

2.4. Fabrication of $CuFe_2O_4$ ND@RGO composite modified MSPE

The $CuFe_2O_4$ ND@RGO nanocomposite (1 mg mL^{-1}) was re-dispersed into a water/ethanol (1 : 3) solvent mixture through ultrasonication for 10 min. Next, 8 μL dispersion of the $CuFe_2O_4$ ND@RGO composite was dropped on the working electrode of a clean MSPE and dried under ambient conditions. Modified GO and unmodified MSPE were prepared for control experiments.

This journal is © the Partner Organisations 2018

Published on 21 February 2018. Downloaded by KING SAUD UNIVERSITY LIBRARIES on 04/04/2018 08:24:15.

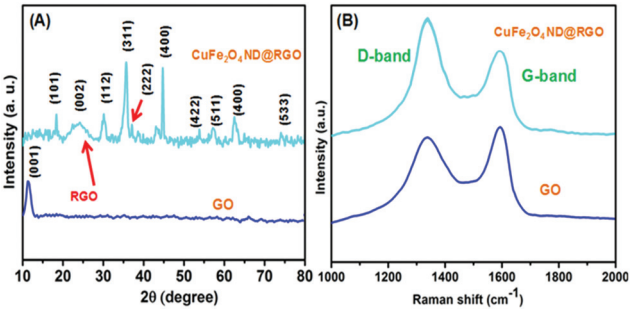

Fig. 1 XRD pattern (A) and Raman spectra (B) of GO and the $CuFe_2O_4$ ND@RGO composite.

3. Results and discussion

3.1. Characterization of a $CuFe_2O_4$ ND@RGO composite

The XRD patterns of GO and the $CuFe_2O_4$ ND@RGO composite are shown in Fig. 1A. The formation of GO was confirmed by the XRD pattern, as it displayed a characteristic peak at 11.7° corresponding to the (001) planes of GO.[29–31] The spectra of the $CuFe_2O_4$ ND@RGO composite featured with several additional diffraction peaks located at 2θ of 18.05, 30.11, 35.29, 36.02, 44.59, 54.12, 58.14, 64.63, and 75.39° are indexed to the (111), (220), (311), (222), (400), (422), (511), (440), and (551) planes, respectively. These peaks are matched well with that of the cubic spinel structured $CuFe_2O_4$ ($CuFe_2O_4$-JCPDS No. 85-1326); thus XRD studies verify the observed particles as $CuFe_2O_4$ particles. The characteristic peak of GO at 11.7° disappeared, while a new peak was observed at 23.85°, which stands for the (002) planes of RGO.[20,32–34] Thus, GO was reduced to RGO during the ascorbic acid incorporated condensation process.

To explore the structural difference of GO (a), and the $CuFe_2O_4$ ND@RGO composite (b), their Raman spectra were analysed (Fig. 1B), where the relative D-band and G-band peak intensities (ID/IG) reflect the general density of defects in the sp^2 lattice. The Raman spectrum displays two sharp bands at 1328 and 1595 cm^{-1}, which are correlated to the D band (A1g mode) and G band (E2g mode), respectively.[35] The ID/IG intensity ratio was significantly increased in $CuFe_2O_4$ ND@RGO over the ratio of GO. A reasoned explanation is the formation of graphitic domains because of GO conversion to RGO and the generation of numerous edge sites on the sheets that causes a decrease in the average size of the in-plane sp^2 domain.[36,37]

The TEM image of GO (Fig. 2A) displays porous interconnected networks of thin sheets. The TEM image of the $CuFe_2O_4$ ND@RGO composite exposed the uniformly distributed spherical-like $CuFe_2O_4$ nanodots entrapped by curled and thin sheets of porous RGO (Fig. 2B and C). As evident from the TEM image, the networks of porous RGO sheets hierarchically interconnect the nanodots. There might be electrostatic interactions between $CuFe_2O_4$ dots and RGO sheets. The EDX profile of the $CuFe_2O_4$ ND@RGO composite presents the

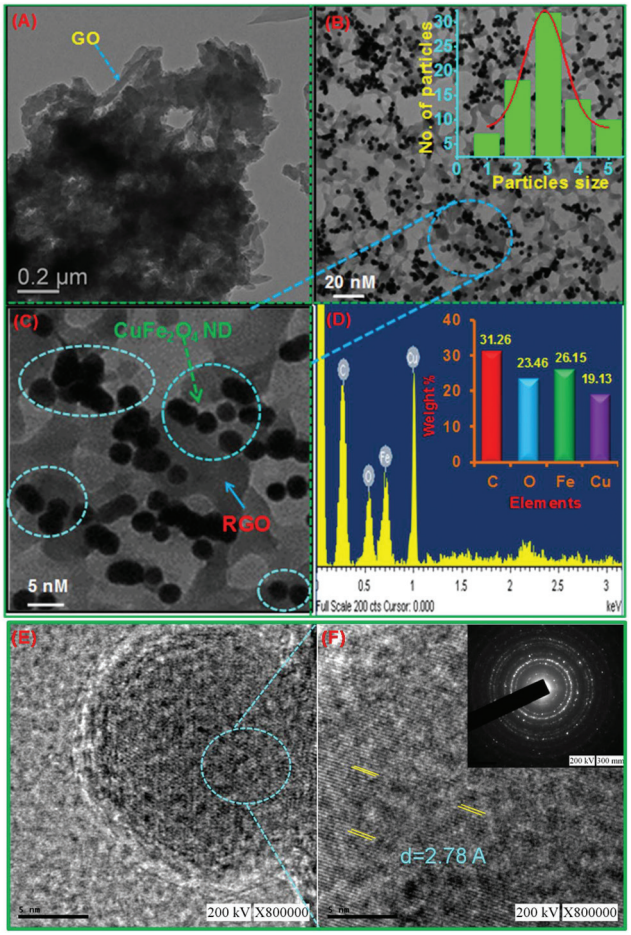

Fig. 2 TEM images of GO (A) and the $CuFe_2O_4$ ND@RGO composite (B, and C); the inset in (B) shows the histogram of $CuFe_2O_4$ ND of $CuFe_2O_4$ ND@RGO. EDX spectrum of $CuFe_2O_4$ ND@RGO (D). HR-TEM images of $CuFe_2O_4$ ND@RGO crystalline phase measurement (E and F); the inset in (F) displays the corresponding SAED pattern.

signals corresponding to carbon, oxygen, copper, and iron with weight percentages of 31.26, 23.46, 26.15 and 19.13, respectively, which shows the elemental composition of the composite (Fig. 2D). Furthermore, HR-TEM and SAED patterns of $CuFe_2O_4$ ND@RGO were used to investigate the crystalline phase of $CuFe_2O_4$. The closer observation of lattice fringes in HR-TEM indicates the cubic spinel structure of $CuFe_2O_4$ (Fig. 2E and F).[38] The selected area electron diffraction (SAED) pattern of $CuFe_2O_4$@RGO featured with typical diffraction rings (111), (220), (311), (222), (400), (422), (511), (440), and (551) is consistent with previous reports (Fig. 2F inset).[39]

TGA analysis is a useful tool to study the thermal stability and composition of the composite. The TGA curve of the $CuFe_2O_4$@RGO nanocomposite under an air atmosphere is given in Fig. 3B. It demonstrates that $CuFe_2O_4$ particles are stable. The $CuFe_2O_4$@RGO has two mass losses at temperatures of 300 and 550 °C, respectively, which can be assigned to the degradation of RGO and $CuFe_2O_4$. According to the weight loses of $CuFe_2O_4$@RGO, the amounts of $CuFe_2O_4$ and RGO in

Published on 21 February 2018. Downloaded by KING SAUD UNIVERSITY LIBRARIES on 04/04/2018 08:24:15.

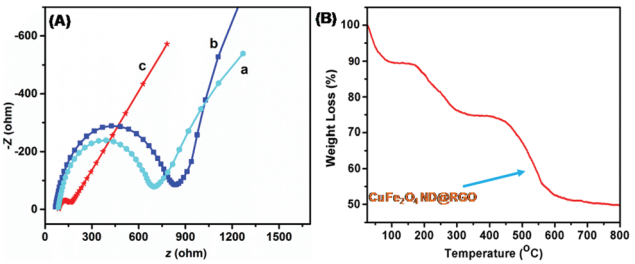

Fig. 3 (A) Nyquist plots of bare MSPE (a), GO/MSPE (b), and $CuFe_2O_4$ ND@RGO/MSPE (c) measured in the frequency range from 100 kHz to 1 Hz in 0.001 M $[Fe(CN)_6]^{3-/4-}$ in 0.1 M KCl electrolyte. (B) TGA curve of the $CuFe_2O_4$ ND@RGO nanocomposite.

the $CuFe_2O_4$@RGO were estimated to be 52.0%, and 48.0%, respectively.[40]

3.2. Electrochemical conductive behaviour of the $CuFe_2O_4$ ND@RGO composite

Electrochemical impedance spectroscopy (EIS) is a useful method for probing the features of nanomaterial modified electrodes. Fig. 3(A) shows the EIS (Nyquist) plots of bare MSPE (a), GO/MSPE (b), and $CuFe_2O_4$ ND@RGO/MSPE (c) recorded in 0.1 M KCl containing 5 mM $[Fe(CN)_6]^{3-/4-}$. It is known that the diameter of the semicircle in the Nyquist plot can be used as a measure of R_{ct} (charge transfer resistance).[41] The R_{ct} values obtained at various modified MSPEs follow the order: $CuFe_2O_4$ ND@RGO/MSPE (97 Ω) < bare MSPE (610 Ω) < GO/MSPE (726 Ω).[42] The $CuFe_2O_4$ ND@RGO composite modified electrode has a low semicircle diameter which indicates a low electrical resistance at the $CuFe_2O_4$ ND@RGO/MSPE electrode/electrolyte interface. In other words, $CuFe_2O_4$ ND@RGO significantly improves the electrical conductivity of the interface over control electrodes which is useful in making electrochemical sensors.

3.3. Electrocatalysis of 3-NT at the $CuFe_2O_4$ ND@RGO composite

The electrocatalytic performance of unmodified, GO, and $CuFe_2O_4$ ND@RGO composite modified electrodes towards 25 μM 3-NT has been assessed using cyclic voltammograms (CV). The CVs were performed in PB (pH = 7), while the scan rate was held at 0.05 V s^{-1} (Fig. 4A). At the $CuFe_2O_4$ ND@RGO modified electrode, a sharp reduction peak was obtained at −0.54 V, which is due to the cathodic conversion of the nitro group of 3-NT into hydroxylamine (eqn (1), Scheme 2). In addition, a pair of redox couples was observed at a formal potential of −0.02 V, which can be correlated to the reversible conversion of hydroxylamine into a nitroso derivate (eqn (2), Scheme 2). Compared to the GO modified and unmodified electrodes, $CuFe_2O_4$ ND@RGO/MSPEs have shown significantly improved electrocatalytic ability towards 3-NT, which is evident from the observed minimized overpotential (−0.54 V) and enhanced peak currents. There might be good synergetic catalytic effect between $CuFe_2O_4$ ND and RGO in the composite as this is the case for many established graphene based nanocomposites. As a result, the nanocomposite encompassed high electronic mobility, high catalytic cavity centres, good conductivity, and large surface area as well.

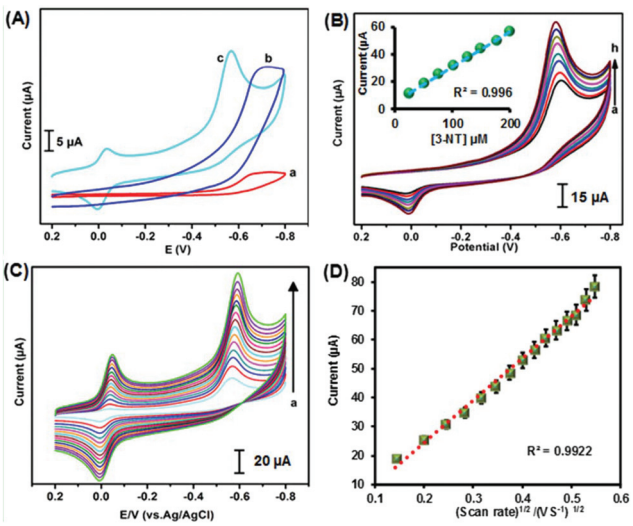

Fig. 4 (A) CVs obtained at unmodified (a), GO (b), and $CuFe_2O_4$ ND@RGO (c) composite modified electrodes in PB (pH 7) containing 25 μM 3-NT. Scan rate = 0.05 V s^{-1}. (B) The response of the $CuFe_2O_4$ ND@RGO modified electrode in 0.1 M PB (pH 7) towards different concentrations of 3-NT. Inset: Linear calibration curve for peak current *vs.* [3-NT]. (C) The $CuFe_2O_4$ ND@RGO modified electrode in PB (pH 7) containing a fixed concentration of 3-NT (25 μM) at different scan rates. (D) Plot of peak current *vs.* square root of the scan rate.

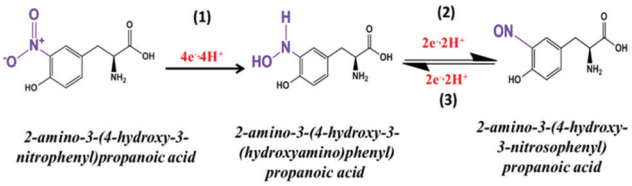

Scheme 2 A proposed electrochemical mechanism of 3-NT.

Fig. 4B shows the CVs of the $CuFe_2O_4$ ND@RGO/MSPE in response to different concentrations of 3-NT. The cathodic peak current (I_{pc}) linearly increases as the concentration of 3-NT increases, which indicates efficient electrocatalysis. The plot between peak current and concentration of 3-NT displays good linearity in the range of 50 to 400 μM by the CV method (inset to Fig. 4B). The respective regression equation is,

$$I_{pc}\ (\mu A) = 0.592\ (\mu A/\mu M)\ [3\text{-NT}] + 4.758\ (R^2 = 0.996).$$

Fig. 4C displays the effect of scan rate on the reduction peak current of 3-NT. The study was conducted by applying different scan rates from 0.2 to 0.2 V s^{-1}. It is obvious that accompanying the increase of scan rates, both the reduction (peak 1, −0.58 V), and redox peaks (peak-2, at 0.01 and second reduction peak 3, at −0.05 V) are increased (Scheme 2). Moreover, with the increase of the scan rate, the cathodic

This journal is © the Partner Organisations 2018

Published on 21 February 2018. Downloaded by KING SAUD UNIVERSITY LIBRARIES on 04/04/2018 08:24:15.

peaks shift to a more negative region. Fig. 4D shows that the plot of reduction peak current and square root of scan rates displays good linearity, which indicates the diffusion controlled electrocatalysis at the modified electrode. The regression equation for the square root of scan rate *vs.* peak current is,

$$I_{3\text{-NT}}\ (\mu\text{A}) = 145.69\text{–}4.5676\ \nu^{1/2}\ ((\text{V s}^{-1})^{1/2})\ (R^2 = 0.992).$$

3.4. Amperometric determination of 3-NT

Fig. 5A and B display the amperometric response of the $CuFe_2O_4$ ND@RGO composite modified electrode towards different concentrations of 3-NT injected in PB (pH 7) at constant intervals. For each addition, a quick and stable amperometric response was observed. The amperometric current was increased linearly as the concentrations of 3-NT were increased. A plot between concentration of 3-NT and peak current displays good linearity with a wide linear range from 4.25 nM to 1347.5 μM (Fig. 5C and D). The sensitivity was calculated to be 8.515 (±0.26) μA μM^{-1} cm^{-2}, while the limit of detection (LOD) was calculated to be 25.14 pM. The LOD was calculated using the equation, LOD = $3\sigma/S$, where σ is the standard deviation of the 10 blank currents and S is the sensitivity. Thus, low levels of 3-NT up to 25.14 pM can be detected and quantified in unknown samples using the $CuFe_2O_4$ ND@RGO composite modified electrode. The ultra-low detection limit obtained by our method surpassed the detection limits of many existing analytical methods.[8–11]

The selectivity of the modified electrode towards 3-NT detection in the presence of potential possible interferents such as, dopamine, uric acid, ascorbic acid, folic acid, glucose, H_2O_2, Hg^{2+}, Cu^{2+}, Fe^{2+}, Cl^-, and Cr^{2+}, has been studied. 5 μM

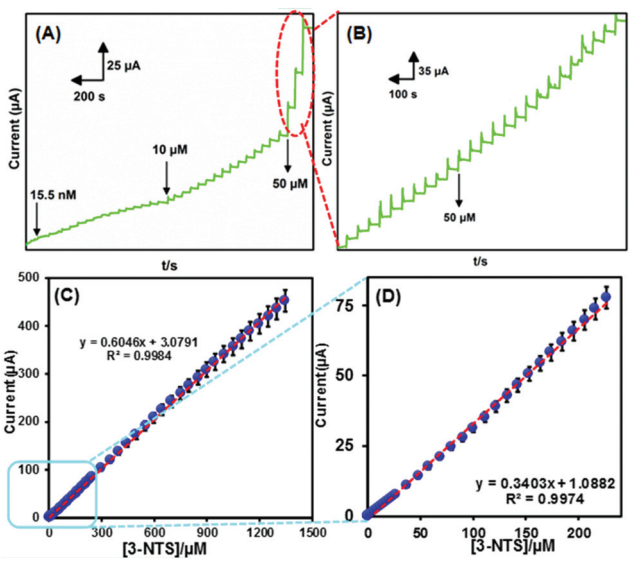

Fig. 5 (A, and B) show the amperometric response obtained at the $CuFe_2O_4$ ND@RGO composite modified electrode in PB (pH 7) containing the additions of 3-NT at 1200 RPM. (C, and D) Response current (μA) *vs.* [3-NT]/μM.

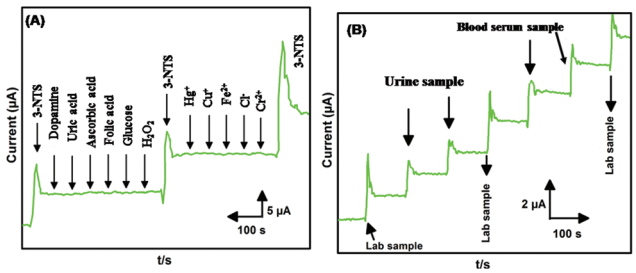

Fig. 6 (A) Amperometric curve of the $CuFe_2O_4$ ND@RGO modified electrode towards 5 μM 3-NT and 50-fold excess concentrations of interfering compounds. (B) Real sample analysis: amperometric curve of the $CuFe_2O_4$ ND@RGO modified electrode towards 3-NT spiked human urine and blood samples.

of 3-NT and 50-fold excess concentrations of interfering compounds were used for the selectivity test. As shown in Fig. 6A, the modified electrode delivered a good current response to 3-NT. However, negligible responses were observed for the tested interferents, which suggests the good selectivity of the electrode towards 3-NT among other compounds.

3.5. Stability, repeatability and reproducibility studies

In order to determine the storage stability of the $CuFe_2O_4$ ND@RGO modified electrode, its electrocatalytic response to 5 μM 3-NT was monitored every day. The electrode was kept stored in PB (pH 7) at 4 °C when not in use. The modified electrode presented a well-defined catalytic response during two weeks of the storage period. About 96.87% of the initial response current was retained over two weeks of its continuous use, which reveals good storage stability. Next, repeatability and reproducibility were tested in phosphate buffer (pH 7) containing 5 μM 3-NT. The modified electrode exhibits appreciable repeatability with a relative standard deviation of 3.74% for five repetitive measurements carried out using a single electrode. The electrode shows good reproducibility of 3.44% for the five independent measurements carried out in five different electrodes.

3.6. Real sample analysis

The practical applicability of the method was demonstrated in biological fluids such as human urine and blood samples (Fig. 6B). The real samples were used without any pre-treatment. The biological samples are 3-NT free; a known amount of 3-NT was spiked prior to analysis. The spiked 3-NT concentrations were 5 and 10 μM. Next, the amount of 3-NT spiked in the samples was tested using the $CuFe_2O_4$ ND@RGO composite modified electrode. The added, found and recovery values are presented in Table 1. The recovery values are in the acceptable range of 97.4 to 99.6%, and hence the $CuFe_2O_4$ ND@RGO composite modified electrode has good practical feasibility. We established a sensitive electrochemical detection method for the quantification of 3-NT in biological fluids, and this analysis method can be correlated to the oxidative stress levels of the body.

Published on 21 February 2018. Downloaded by KING SAUD UNIVERSITY LIBRARIES on 04/04/2018 08:24:15.

Table 1 Determination of spiked 3-NT in biological samples using the $CuFe_2O_4$ ND@RGO composite modified electrode

Samples	Added (μM)	Found (μM)	Recovery (%)	RSD[a] (%)
Urine	5	4.98	99.6	1.26
	10	9.85	98.5	2.47
Blood serum	5	4.91	98.2	2.56
	10	9.74	97.4	3.24

[a] RSD (Relative Standard Deviation) of three individual experiments.

4. Conclusions

A highly sensitive, selective, reproducible and stable electrochemical sensing platform was described for the detection of an oxidative stress biomarker using a $CuFe_2O_4$ ND@RGO nanocomposite. A facile green method was reported for the production of $CuFe_2O_4$ ND@RGO and the formation of the nanocomposite was verified by morphological, elemental and spectroscopic methods. Voltammetric studies revealed the improved electrocatalysis of 3-NT at the $CuFe_2O_4$ ND@RGO modified electrode. Excellent analytical parameters such as wide linear ranges (4.25 nM–1347.5 μM) and low limit of detection (25.14 pM) have been achieved for amperometric 3-NT detection. The practicality of the modified electrode had been successfully verified in biological fluids; thus the method holds potential use to understand the oxidative stress levels of the body.

Conflicts of interest

There are no conflicts to declare.

Acknowledgements

The authors extend their appreciation to the Deanship of Scientific Research at King Saud University for funding this work through research group no. RG-195. This work was supported by the Ministry of Science and Technology, Taiwan (MOST 106-2113-M-027-003).

References

1 J. W. Baynes, *Diabetes*, 1991, **40**, 405–412.
2 K. Hensley, M. L. Maidt, Z. Yu, H. Sang, W. R. Markesbery and R. A. Floyd, *J. Neurosci.*, 1998, **18**, 8126–8132.
3 P. Jenner, *Ann. Neurol.*, 2003, **53**, S26–S38.
4 M. F. Beal, *Ann. N. Y. Acad. Sci.*, 2003, **991**, 120–131.
5 J. Himmelfarb, P. Stenvinkel, T. A. Ikizler and R. M. Hakim, *Kidney Int.*, 2002, **62**, 1524–1538.
6 M. Jaiswal, N. F. LaRusso, L. J. Burgart and G. J. Gores, *Cancer Res.*, 2000, **60**, 184–190.
7 M. Ichinose, H. Sugiura, S. Yamagata, A. Koarai and K. Shirato, *Am. J. Respir. Crit. Care Med.*, 2000, **162**, 701–706.
8 Y. Ishii, M. Iijima, T. Umemura, A. Nishikawa, Y. Iwasaki, R. Ito, K. Saito, M. Hirose and H. Nakazawa, *J. Pharm. Biomed. Anal.*, 2006, **41**, 1325–1331.
9 L. A. MacMillan-Crow, J. P. Crow and J. A. Thompson, *Biochemistry*, 1998, **37**, 1613–1622.
10 L. Denoroy and S. Parrot, *Sep. Purif. Rev.*, 2017, **46**, 108–151.
11 M. Jaroš, K. Včeláková, I. Zusková and B. Gaš, *Electrophoresis*, 2002, **23**, 2667–2677.
12 M. Govindasamy, S.-M. Chen, V. Mani, A. Sathiyan, J. P. Merlin, F. M. Al-Hemaid and M. A. Ali, *RSC Adv.*, 2016, **6**, 100605–100613.
13 Z. Zhu, Y. Su, J. Li, D. Li, J. Zhang, S. Song, Y. Zhao, G. Li and C. Fan, *Anal. Chem.*, 2009, **81**, 7660–7666.
14 M. Mazloum-Ardakani, B. Ganjipour, H. Beitollahi, M. K. Amini, F. Mirkhalaf, H. Naeimi and M. Nejati-Barzoki, *Electrochim. Acta*, 2011, **56**, 9113–9120.
15 Z.-H. Sheng, X.-Q. Zheng, J.-Y. Xu, W.-J. Bao, F.-B. Wang and X.-H. Xia, *Biosens. Bioelectron.*, 2012, **34**, 125–131.
16 D. S. Su, S. Perathoner and G. Centi, *Chem. Rev.*, 2013, **113**, 5782–5816.
17 C. Wang, J. Du, H. Wang, C. E. Zou, F. Jiang, P. Yang and Y. Du, *Sens. Actuators, B*, 2014, **204**, 302–309.
18 X. Kang, J. Wang, H. Wu, I. A. Aksay, J. Liu and Y. Lin, *Biosens. Bioelectron.*, 2009, **25**, 901–905.
19 J. J. Gooding, *Electrochim. Acta*, 2005, **50**, 3049–3060.
20 M. Zhou, Y. Zhai and S. Dong, *Anal. Chem.*, 2009, **81**, 5603–5613.
21 Y. Guo, S. Guo, J. Ren, Y. Zhai, S. Dong and E. Wang, *ACS Nano*, 2010, **4**, 4001–4010.
22 X.-C. Dong, H. Xu, X.-W. Wang, Y.-X. Huang, M. B. Chan-Park, H. Zhang, L.-H. Wang, W. Huang and P. Chen, *ACS Nano*, 2012, **6**, 3206–3213.
23 M. Gong, Y. Li, H. Wang, Y. Liang, J. Z. Wu, J. Zhou, J. Wang, T. Regier, F. Wei and H. Dai, *J. Am. Chem. Soc.*, 2013, **135**, 8452–8455.
24 A. E. Vilian, V. Mani, S.-M. Chen, B. Dinesh and S.-T. Huang, *Ind. Eng. Chem. Res.*, 2014, **53**, 15582–15589.
25 J. Tian, Q. Liu, A. M. Asiri, A. O. Al-Youbi and X. Sun, *Anal. Chem.*, 2013, **85**, 5595–5599.
26 B. Šljukić, C. E. Banks and R. G. Compton, *Nano Lett.*, 2006, **6**, 1556–1558.
27 Y. Zhu, S. Murali, W. Cai, X. Li, J. W. Suk, J. R. Potts and R. S. Ruoff, *Adv. Mater.*, 2010, **22**, 3906–3924.
28 D. A. Dikin, S. Stankovich, E. J. Zimney, R. D. Piner, G. H. Dommett, G. Evmenenko, S. T. Nguyen and R. S. Ruoff, *Nature*, 2007, **448**, 457–460.
29 D. C. Marcano, D. V. Kosynkin, J. M. Berlin, A. Sinitskii, Z. Sun, A. Slesarev, L. B. Alemany, W. Lu and J. M. Tour, *ACS Nano*, 2010, **4**, 4806–4814.
30 L. Chen, Y. Tang, K. Wang, C. Liu and S. Luo, *Electrochem. Commun.*, 2011, **13**, 133–137.

 This journal is © the Partner Organisations 2018

Published on 21 February 2018. Downloaded by KING SAUD UNIVERSITY LIBRARIES on 04/04/2018 08:24:15.

31 D. R. Dreyer, S. Park, C. W. Bielawski and R. S. Ruoff, *Chem. Soc. Rev.*, 2010, **39**, 228–240.
32 V. Krishnan, R. K. Selvan, C. O. Augustin, A. Gedanken and H. Bertagnolli, *J. Phys. Chem. C*, 2007, **111**, 16724–16733.
33 H. Teymourian, A. Salimi and S. Khezrian, *Biosens. Bioelectron.*, 2013, **49**, 1–8.
34 C. Zhu, S. Guo, Y. Fang and S. Dong, *ACS Nano*, 2010, **4**, 2429–2437.
35 G. K. Ramesha and S. Sampath, *J. Phys. Chem. C*, 2009, **113**, 7985–7989.
36 C. Gómez-Navarro, R. T. Weitz, A. M. Bittner, M. Scolari, A. Mews, M. Burghard and K. Kern, *Nano Lett.*, 2007, **7**, 3499–3503.
37 X. Li, H. Wang, J. T. Robinson, H. Sanchez, G. Diankov and H. Dai, *J. Am. Chem. Soc.*, 2009, **131**, 15939–15944.
38 Y. Wang, H. Zhao, M. Li, J. Fan and G. Zhao, *Appl. Catal., B*, 2014, **147**, 534–545.
39 V. Manikandan, A. Vanitha, E. R. Kumar and J. Chandrasekaran, *J. Magn. Magn. Mater.*, 2017, **423**, 250–255.
40 A. V. Nakhate and G. D. Yadav, *ChemistrySelect*, 2017, **2**, 7150–7159.
41 M. Levi and D. Aurbach, *J. Phys. Chem. B*, 1997, **101**, 4630–4640.
42 E. Casero, A. Parra-Alfambra, M. Petit-Domínguez, F. Pariente, E. Lorenzo and C. Alonso, *Electrochem. Commun.*, 2012, **20**, 63–66.